PHYSICS OF FLUIDS **26**, 084106 (2014)

Influence of confinement on the oscillations of a free cylinder in a viscous flow

Luciano Gianorio,[1,a)] Maria Veronica D'Angelo,[1,b)] Mario Cachile,[1,c)] Jean-Pierre Hulin,[2,d)] and Harold Auradou[2,e)]
[1]*Grupo de Medios Porosos, Facultad de Ingeniería, Paseo Colon 850, 1063 Buenos Aires, Argentina and CONICET, Buenos Aires, Argentina*
[2]*Univ Paris-Sud, CNRS, F-91405. Lab FAST, Bât 502, Campus Univ, Orsay F-91405, France*

(Received 27 June 2013; accepted 2 August 2014; published online 25 August 2014)

We demonstrate and study experimentally two instabilities of a horizontal free cylinder in a vertical viscous Hele-Shaw flow; we show that they depend critically on the confinement of the flow with a different influence of transverse and lateral confinement characterized respectively by the ratios of the diameter (resp. the length) of the cylinder to the gap (resp. the width) of the cell. The onset of the instabilities depends largely on the transverse confinement: for a parameter between 0.4 and 0.6, one observes *transverse* horizontal *oscillations* of the cylinder perpendicular to the walls: their frequency is constant with the lateral and transverse confinements at a given cylinder velocity. This instability is shown to be locally two-dimensional and controlled by the *local* relative velocity between the cylinder and the fluids: it occurs down to Reynolds numbers based on the cell gap $\simeq 15$, far below the corresponding 2D vortex shedding thresholds (150−250) for fixed cylinders between parallel planes. Above transverse confinements of the order of 0.55, we observe a *fluttering* motion with periodic oscillations of the tilt angle of the cylinder from the horizontal and of its horizontal position: their frequency decreases strongly as the lateral confinement increases but is independent of the transverse confinement and the cylinder velocity.
 [http://dx.doi.org/10.1063/1.4893342]

I. INTRODUCTION

Elongated particles moving in confined flows are encountered in many natural systems and industrial applications such as the transport or propulsion of fibers or long bio-particles in microfluidic channels.[1] Another example is the addition of fibers to prevent the backflow of proppant particles during the injection of fracturing fluids in reservoir rocks[2]; finally, fiber sensors may be used in order to perform underground *in situ* measurements of, for instance, local temperatures or fluid compositions for oil engineering or hydrogeological purposes.[3–5] In such applications, the fibers need to move into flows channels with an aperture of the order of the fiber diameter so that strong confinement effects may be expected.

In connection with the latter example, previous experiments[6] studied the transport of long flexible fibers by a viscous flow in transparent rough model fractures comparable to those in real rocks. While, for flat smooth walls, the fibers remain straight and parallel to the flow, in the rough case, they display complex shapes and their orientation with respect to the local flow varies. The interaction with the walls may be strong, leading to undesirable local pinning: a key issue is whether the fiber remains centered in the gap between the walls of the cell which minimizes the interaction or

[a)]Electronic mail: luchogiano@gmail.com
[b)]Electronic mail: vdangelo@fi.uba.ar
[c)]Electronic mail: mcachil@fi.uba.ar
[d)]Electronic mail: hulin@fast.u-psud.fr
[e)]Electronic mail: auradou@fast.u-psud.fr

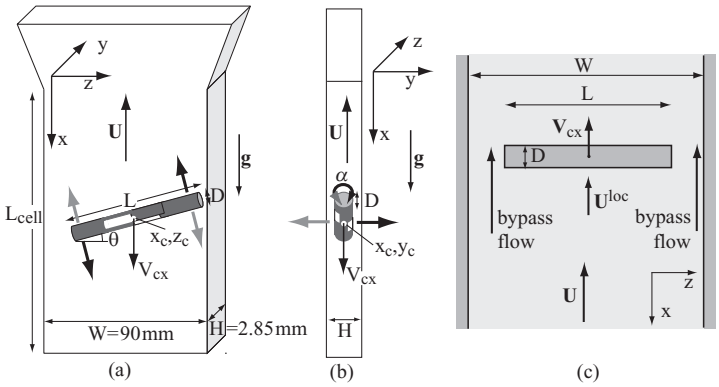

FIG. 1. Schematic views of the experimental setup. (a) Front view and (b) side view. Thick oblique grey and black arrows on (a) represent the motion corresponding to fluttering oscillations. Thick horizontal and rounded arrows on (b) represent the displacements and rotations for transverse oscillations. (c) Schematic view of the flow distribution around the cylinder.

whether it touches these walls. Instabilities of the motion of the cylinder play a very important part in these processes either by bringing the fibers in contact with the walls or, instead, by depinning them. Another potential application of these oscillatory instabilities is to induce mixing in viscous flows in small channels such as those used in microfluidic devices.

In view of the complexity of this problem, we study as a first step the better controlled instabilities of straight rigid cylinders representing sections of a long fiber and moving freely inside a vertical Hele-Shaw cell with flat parallel walls (Fig. 1). The cylinder is perpendicular to the flow which was found to be the most favorable configuration for the development of instabilities (no oscillations occurred for free or tethered cylinders parallel to the flow).

The objective of the present paper is to show that the appearance of these instabilities and their characteristics are largely due to the confinement of the flow, characterized in the following by the ratios of the cylinder length to the cell width and of its diameter to the gap. Moreover, these instabilities display several specific new characteristics differing from those observed on fixed similar objects or in unconfined flows.

A first kind of previous studies in similar systems dealt with the hydrodynamic forces on static cylinders submitted to a flow between parallel plates or in a rectangular channel.[7–9] Most investigations of hydrodynamic instabilities in similar confined geometries studied vortex shedding behind fixed cylinders.[10–15] Studies of moving cylinders were often restricted to stable displacements.[16–20] Finally, oscillatory paths observed during the sedimentation of solid bodies in a viscous fluid[21–24] and periodic fluttering motions of plates falling in air[25–27] are generally analyzed without considering the effect of confinement.

Using the present configuration (see Fig. 1), we reported previously 2*D* numerical simulations and experiments on horizontal cylinders ($\theta = 0$) in a vertical flow; these experiments used a nearly 2*D* flow configuration with a length L ($\gg D$) of the cylinders close to the width W of the cell. The cylinders were tethered[28] or completely free[29] and could move respectively only in the y direction or in both the x and y directions. In both cases, oscillations of the cylinder in the direction y were observed and we refer to them in the following as *transverse oscillations*. Moreover, the rolling angle α of a free cylinder oscillates at the same time as its location along y and at the same frequency.[29] More generally, displacements along y will be called "transverse," along z "lateral," and along x "vertical."

In these nearly 2*D* configurations, the global flow velocity U is representative of the velocity over the cylinder (there are no bypass flows at the ends); for a tethered cylinder or a free one with a zero vertical velocity ($V_{cx} = 0$), one can then define the Reynolds number as $Re = UH/\nu$ (H = cell gap). In the tethered case,[28] the threshold Re for the transverse oscillations was of the order of 19 and they were observed down to $Re \simeq 20$ for a free cylinder.[29] This is much lower than the thresholds predicted by 2*D* numerical simulations[10,12] of vortex shedding behind fixed cylinders between parallel planes: still using the cell gap as the characteristic length, these values range from

$Re = 150$ for $D/H = 0.7$ to 250 for $D/H = 0.5$. Moreover, for tethered cylinders of high density $\rho_s > 4 \times 10^3$ kg/m^3, $2D$ numerical simulations in the same geometry[28] show that as Re increases further above the threshold, the transverse oscillations first vanish and, then, smaller oscillations due to vortex shedding occur at still higher values $Re \gtrsim 110$. The two types of oscillations correspond therefore likely to different processes.

In this paper, we study the changes of the characteristics of this instability and whether new ones appear when the length L of the cylinder is smaller than W so that the flow geometry is no longer two dimensional. The study has been performed down to small normalized lengths of the cylinder ($L/W = 0.055$) and for several normalized diameters D/H (L/W and D/H characterize respectively the lateral and the transverse confinement).

An important consequence of the reduced length is that the cylinder can move sideways parallel to the z axis with a global amplitude of the order of $L - W$. As a result, a *fluttering instability* inducing oscillations of both the coordinate z of the center of mass of the cylinder and of the angle θ with the horizontal may appear: it is observed either alone or combined with the former, transverse, instability. A second consequence is that bypass flows appear between the ends of the cylinder and the cell boundaries (Fig. 1(c)). In the simple case of a free cylinder of zero vertical velocity V_{cx} or of a tethered cylinder the local relative velocity of the cylinder and the flow no longer corresponds to the global flow velocity U but to a local velocity U^{loc} ($|U^{loc}| < |U|$). As will be shown in Sec. IV A, the onset and the characteristics of the transverse oscillations are likely determined by U^{loc} rather than by U.

For free cylinders, in the general case ($L < W$, $V_{cx} \neq 0$), the meaningful velocity is neither U^{loc} nor V_{cx} but a local relative velocity V_r^{loc} which is a combination of the two. The relevant Reynolds number is then defined as $Re^{loc} = V_r^{loc} H/\nu$. A problem is that neither U^{loc} nor V_r^{loc} are measurable directly, except if $L \to W$, in which case $U^{loc} = U$ (in this limit, transverse oscillations still take place while the fluttering motion gets blocked by steric interactions with the side walls). Practically, we estimate V_r^{loc} (and Re^{loc}) by combining measurements using free cylinders of different lengths and same diameter (see Sec. IV A).

In the following, we identify first for free cylinders the domains of observation of the *transverse* and *fluttering* instabilities as a function of the confinement parameters L/W and D/H. Next, the relation between the velocities V_{cx} and U is investigated experimentally as a function of L/W for a constant diameter. This provides important information on the values of the local velocities U^{loc} and V_r^{loc} which determine the onset and frequency of the instabilities and on the variation of Re^{loc}. The results are then generalized to other diameters and the variation of the frequency f of the transverse oscillations is studied as a function of L/W and D/H: these data are interpreted in relation with the variations of V_{cx} with U for the same cylinders. Varying the viscosity of the flowing fluid provides the variation of the Strouhal number with Re^{loc} which is then compared to experimental and numerical results obtained previously for tethered cylinders. Finally, the characteristics of the fluttering instability are studied as a function of L/W and of the cylinder velocity for different ratios D/H and are compared to those of the transverse oscillations.

II. EXPERIMENTAL SETUP AND PROCEDURE

The experimental setup has been described in Ref. 29 and is shown in Fig. 1. The length L_{cell}, width W and gap H of the Hele-Shaw cell are, respectively: 290, 90, and 2.85 mm. The flowing fluids are water-glycerol or water-salt-glycerol solutions. Their physical properties are listed in Table I. All water-salt-glycerol solutions (WGS) have the same density, allowing for a specific study of the influence of the viscosity. The flow rate varies between 0 and 400 ml/mn (corresponding to $-25 \leq U \leq 0$ mm/s): U is negative for an upward flow velocity since the vertical axis x is oriented downward. Here, the flow velocities (U, U^{loc}) are defined as the corresponding flow rate per unit length along z divided by the gap H.

The top part of the cell has a Y-shape so that the local gap increases from 2.85 to 6 mm over a vertical distance of 48 mm. All the experiments are performed using plexiglas cylinders of density $\rho_s = 1.19 \times 10^3$ kg/m^3. Their lengths range between 5 and 85 mm ($0.055 \leq L/W \leq 0.94$) and their diameter between 1.1 and 2.2 mm ($0.39 \leq D/H \leq 0.77$).

TABLE I. Physical properties of the solutions used in the experiments at a temperature $T = 25°$C. Concentration in weight of glycerol: C; density: ρ_f; and dynamical viscosity: μ.

Name	C (%)	ρ_f (g/cm^3)	μ (mPa s)	μ/μ_{water}
		Water-glycerol solutions		
W	0	0.997	0.89	1
$WG5$	5	1.008	1.01	1.13
$WG10$	10	1.02	1.15	1.29
$WG15$	15	1.032	1.33	1.49
		Water-salt-glycerol solutions		
$WGS5$	5	1.035	1.05	1.18
$WGS10$	10	1.035	1.17	1.31
$WGS15$	15	1.035	1.33	1.49

First, the cylinders are placed horizontally at the top end of the cell and one lets them drift into the constant gap region by reducing the flow rate Q; Q is then adjusted in order to bring the cylinder at the desired initial location. Finally, Q is set to the desired value and kept constant during the measurements.

The displacement of the cylinder is monitored by a digital camera viewing the Hele-Shaw cell from the front: its resolution is 1024 × 768 pixels and the frame rate 30 fps. In order to analyze the rolling motion of the cylinder which accompanies the transverse oscillations,[29] black staggered stripes parallel to its axis have been painted on the central portions. We digitally process the images to determine the cylinder's angle θ with respect to the horizontal, the coordinates (x_c, z_c) of its center of mass, and to estimate the roll angle α. The transverse oscillations of the cylinder in the direction y can be detected visually but cannot be measured quantitatively due to the lack of optical access (Fig. 1): they are therefore characterized by the associated variations of the roll angle α.[29]

III. QUALITATIVE PROPERTIES OF DIFFERENT CYLINDER MOTION REGIMES

The different types of motion of the free cylinder have been identified as a function of the control parameters D, L, and U: D and L were observed to have the largest influence on the results. We have therefore displayed in Fig. 2 a map of the different regimes observed as a function of the dimensionless parameters D/H and L/W.

- For $D/H \lesssim 0.4$, the cylinder remains horizontal and follows a straight stable vertical trajectory with no transverse or lateral oscillations.
- For ratios $0.4 \lesssim D/H \lesssim 0.55$, both the roll angle α and the coordinate y_c transverse to the walls (not measurable in the present experiments) oscillate at a frequency f. Moreover, the vertical displacement δx_c displays small oscillations of frequency $2f$ superimposed over the vertical drift of velocity V_{cx} (Figs. 3(a) and 3(b)). There is no correlated variation of the lateral displacement δz_c and the cylinder remains at a constant low angle from the horizontal ($\theta \simeq 0$). When $D/H \gtrsim 0.55$, or when $L/W = 0.89$ and 0.95 for $D/H = 0.53$, a periodic fluttering motion (described below) is superimposed onto these transverse oscillations (Fig. 2): in the second case, its amplitude is low due to the small clearance between the ends of the cylinder and the side walls.
- For $D/H \gtrsim 0.6$, only the fluttering instability is generally observed. Both the angle θ with the horizontal and the lateral displacement δz_c oscillate at a same frequency f_f significantly lower than f (see Figs. 3(c) and 3(d)); the angle $|\theta|$ reaches an extremal value shortly after the end of the cylinder is closest to one of the sides of the cell. There are, in addition, small oscillations of the roll angle and of the deviation δx_c from the global vertical drift of velocity V_{cx}.

In short, increasing the ratio D/H and, therefore, the transverse confinement results in a transition from stable flow to transverse oscillations and then to a fluttering motion.

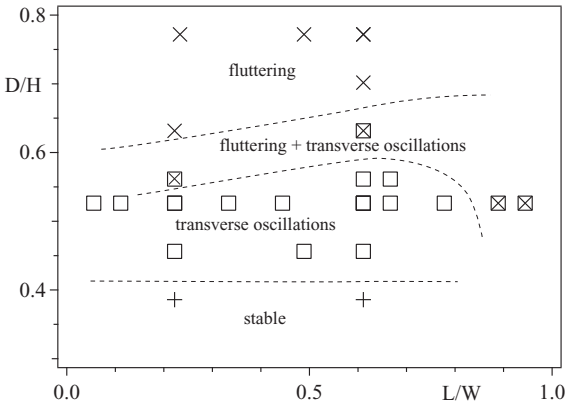

FIG. 2. Different cylinder motion regimes observed as a function of the ratios D/H and L/W for plexiglas cylinders of different lengths and diameters and for the water-glycerol solution $WG10$: straight trajectory (+); transverse oscillation (□); fluttering+transverse oscillation (⊠); and fluttering (×).

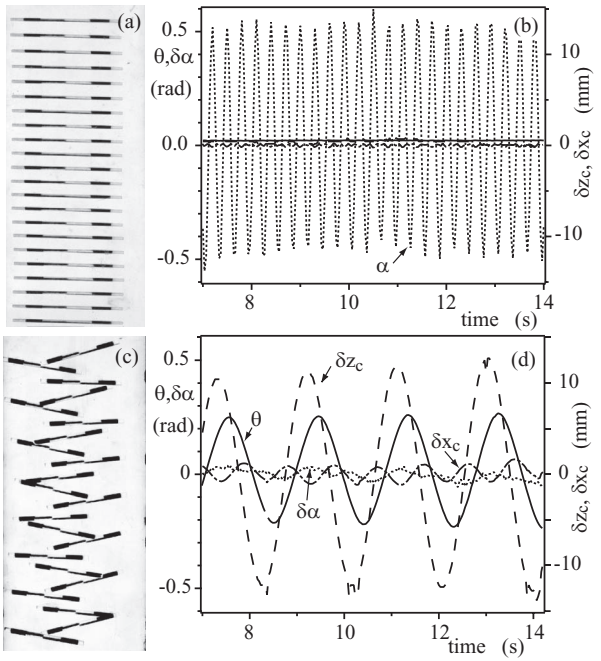

FIG. 3. (a) and (c) Sequences of views taken at constant time intervals Δt. In both cases, the cylinder moves downward. (b) and (d) Time variations in the same experiments of geometrical parameters characterizing the motion of the cylinder: θ = angle of the cylinder axis with respect to the horizontal (continuous line), $\delta\alpha$ = deviation of the roll angle from its mean value (dotted line), δz_c = deviation of the coordinate z of the center of mass of the cylinder from its mean value (dashed line), δx_c = deviation of the coordinate x_c of the center of mass from the mean drift motion (dashed-dotted line). (a) and (b) transverse oscillation regime: $L/W = 0.77$, $D/H = 0.46$, $U = 9.1\,\text{mm s}^{-1}$ ($WG10$ solution), $\Delta t = 1.33\,\text{s}$, field of view: 89 × 195 mm; (c) and (d) fluttering regime: $L/W = 0.49$, $D/H = 0.77$, $U = 7.15\,\text{mm s}^{-1}$ ($WG10$ solution), $\Delta t = 0.66\,\text{s}$, field of view: 78 × 167 mm.

IV. INFLUENCE OF THE TRANSVERSE AND LATERAL CONFINEMENT ON THE GLOBAL MOTION OF FREE CYLINDERS

A. Influence of the cylinder length on the velocity and the Reynolds number

We studied first experimentally the variation of the velocity V_{cx} with the flow velocity U ($-20 \leq U \leq 0\,\text{mm s}^{-1}$) for several dimensionless lengths $0.055 \leq L/W \leq 0.94$ and a constant value of

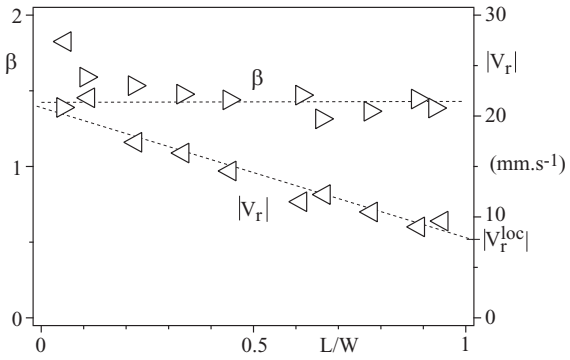

FIG. 4. Variation, as a function of the normalized cylinder length L/W, of the parameters β (▷) and $|V_r|$ (◁) of Eq. (1) for $D/H = 0.53$ ($WG10$ solution).

$D/H = 0.53$. As observed previously,[29] V_{cx} varies linearly with U with

$$V_{cx} = \beta(U - V_r). \tag{1}$$

The parameter $V_r = U - V_{cx}/\beta$ is the global relative velocity of the mean flow and the cylinder. The experimental variations with L/W of β and V_r are plotted in Fig. 4. The slope β is independent of L/W (▷ symbols) with $\beta = 1.4 \pm 0.15$ even when fluttering oscillations are also present. In contrast, $|V_r|$ decreases linearly from 22 to 9 mm s^{-1} as L/W varies from 0.1 to 0.95 (◁ symbols). Only the data point corresponding to the shortest cylinder ($L/W = 0.055$) is significantly above the global trend.

This suggests to generalize the discussion presented in Ref. 29 for $L/W = 1$. In this particular case, the hydrodynamic forces balancing the weight of the cylinder were determined by the combination $V_r = U - V_{cx}/\beta$, constant with U in which β represents the ratio between the coefficients relating the hydrodynamic forces to U and V_{cx}, respectively. For $L < W$, the weight per unit length of the free cylinder is still balanced by the hydrodynamic forces per unit length which must therefore be independent both of L/W and U (or V_{cx}): these forces are then no longer determined by V_r which depends on L/W but by a local relative velocity V_r^{loc} associated to the local flow over the length of the cylinder; like these forces, V_r^{loc} (and Re^{loc}) must be independent of both L/W and U (or V_{cx}). In the limit $L/W \to 1$, V_r and V_r^{loc} must be equal so that one can determine V_r^{loc} (and, therefore Re^{loc}) by extrapolating the variations of V_r with L/W to $L/W = 1$ (Fig. 4).

Physically, this is equivalent to assume that the streamlines are weakly deflected near the ends the cylinder and to break down the flow into two local $2D$ velocity fields (v_x and v_y independent of z): one corresponds to a flow of characteristic velocity $U^{loc} < U$ over the full length of the cylinder and the other to a bypass flow between its ends and the lateral walls (Fig. 1(c)). The velocity $U^{loc} < U$ can be estimated under these assumptions by generalizing Eq. (1) to

$$V_r^{loc} = U^{loc} - V_{cx}/\beta. \tag{2}$$

The lack of variation of β with L/W (including when $L/W \to 1$) justifies using the same value of β in Eqs. (1) and (2): Eq. (2) implies then that U^{loc}, like V_r^{loc} (and unlike U), is also constant with L/W for a given velocity V_{cx}.

In the case of Fig. 4, $V_r^{loc} = -8 \pm 0.3$ mm s^{-1} so that $Re^{loc} = V_r^{loc} H/\nu = 20 \pm 1$. Since Re^{loc} and V_r^{loc} are independent of both L/W and V_{cx}, these values are valid for the whole set of experiments in this figure. The numerical value of U^{loc} depends on V_{cx} (but not on L/W) and becomes equal to V_r^{loc} for $V_{cx} = 0$.

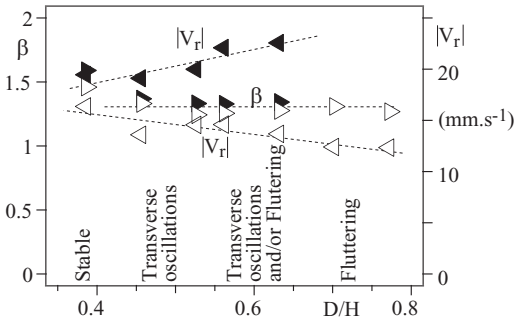

FIG. 5. Experimental variation of the slope β and the velocity V_r with the normalized diameter D/H for two different normalized lengths: $L/W = 0.61$ (open symbols); black; $L/W = 0.22$ (black symbols). Data points correspond to the transverse oscillation regime except for $D/W = 0.39$ (stable regime) and $D/W = 0.7$ and 0.77 (pure fluttering regime). Flowing fluid: $WG10$ solution.

TABLE II. Variations with the ratio D/H of the local relative velocity V_r^{loc} and of the corresponding Reynolds number Re^{loc} ($WG10$ solution).

D/H	V_r^{loc} mm s^{-1}	$Re^{loc} = V_r^{loc} H/\nu$	Type of cylinder motion
0.39	13 ± 1	33 ± 3	Stable
0.46	8 ± 1	20 ± 3	Transverse oscillations
0.53	8 ± 1	20 ± 3	Transverse oscillations
0.56	7 ± 1	18 ± 3	Transverse oscillations
0.63	5 ± 1	12 ± 3	Fluttering

B. Mean velocity and Reynolds number for different diameters

We extend now the results of Secs. IV A and V A by comparing, for two different lengths ($L/W = 0.61$ and $L/W = 0.22$), experiments using cylinders of different diameters ($0.39 \leq D/H \leq 0.77$). Transverse oscillations are observed in the narrower range $0.46 \leq D/H \leq 0.63$ (Fig. 2).

Figure 5 displays the variation with D/H of the parameters β and V_r determined like in Sec. IV A: data points corresponding to pure fluttering ($D/H = 0.7$ and 0.77) or stable ($D/H = 0.39$) regimes are included in the graph and follow the global trend of the other data. The coefficient $\beta = 1.35 \pm 0.1$ is independent of D/H and does not vary at the transition towards the stable or the fluttering regimes. The velocity V_r decreases smoothly by 30% as D/H varies from 0.39 to 0.77 for $L/W = 0.61$ and increases by 15% as D/H varies from 0.39 to 0.63 for $L/W = 0.22$; like for β, there is no visible influence of the transition from a flow regime to another.

For these different ratios D/H, we estimated V_r^{loc} by assuming that, like in Fig. 4, V_r varies linearly with L/W: a linear extrapolation from the experimental determinations of V_r for $L/W = 0.61$ and $L/W = 0.22$ provides then the values of $V_r^{loc} = V_r(L/W = 1)$ listed in Table II. The corresponding Reynolds number Re^{loc} is practically constant between $D/H = 0.45$ and 0.56 at the same low value $\simeq 20$ as in Sec. IV A. The lower values of V_r^{loc} and Re^{loc} for $D/H = 0.63$ may reflect the stronger blockage of the flow.

V. INFLUENCE OF THE TRANSVERSE AND LATERAL CONFINEMENT ON THE TRANSVERSE OSCILLATIONS OF FREE CYLINDERS

A. Influence of the cylinder length on the frequency of the transverse oscillations

We discuss now the influence of the normalized length L/W on the transverse oscillations for the same cylinders as in Sec. IV A ($D/H = 0.53$). For $L/W \leq 0.77$, these oscillations are the only ones taking place and the cylinder remains horizontal (Fig. 2). For $L/W = 0.89$ and 0.94, fluttering is superimposed to them (with a small amplitude due to the high L/W values resulting in strong steric interactions with the walls).

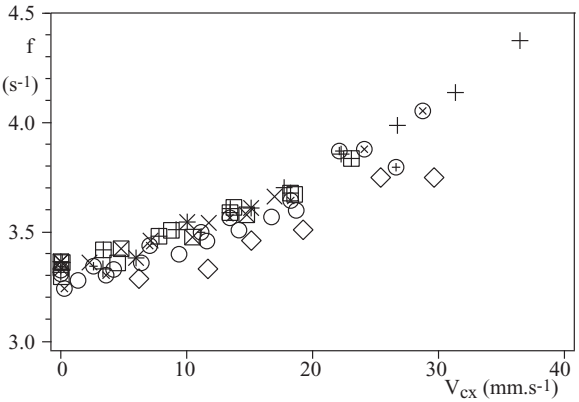

FIG. 6. Experimental variation of the transverse oscillation frequency f as a function of the cylinder velocity V_{cx} for plexiglas cylinders of different lengths and constant diameter $D = 1.5$ mm ($D/H = 0.53$). Flowing fluid: $WG10$ solution. The cylinders used in the experiments are the same as for Fig. 4 and the symbols correspond to the normalized lengths: $L/W = 0.055$ (◊), 0.11 (+), 0.22 (⊗), 0.33 (⊕), 0.44 (⊞), 0.61 (◯), 0.67 (□), 0.77 (×), 0.89 (∗), and 0.94 (⊠)

Figure 6 displays the variations of the frequency of the transverse oscillations with the cylinder velocity V_{cx} for the different ratios L/W. These curves collapse onto a common trend, except for $L/W = 0.055$. For $V_{cx} = 0$, the frequency is $f = 3.3 \pm 0.1$ Hz. Physically, the flow field around the cylinder and, therefore, f are fully determined by the pair of values (V_{cx}, U^{loc}). The fact that f is independent of L/W for a given velocity V_{cx} of a free cylinder confirms, therefore, that U^{loc} is also independent of L/W.

As seen on Fig. 6, the frequency f increases weakly with V_{cx}, i.e., by 15% between $V_{cx} = 0$ and 20 mm s^{-1}. This shows that, while the hydrodynamic forces which balance the weight of the cylinder depend only on V_r^{loc}, f has a more complex dependence on V_{cx} and U^{loc}: more precisely, f depends dominantly of V_r^{loc} but has a residual additional variation with V_{cx}. Moreover, the curves of Fig. 6 corresponding to the two largest values of L/W for which fluttering is superimposed onto the transverse oscillations do not differ from the others: together with the lack of anomaly in the variations of V_r and β at the onset of fluttering, this confirms that the transverse and fluttering oscillations are independent.

B. Transverse oscillation characteristics for cylinders of different diameters

The variation of the frequency f with V_{cx} is plotted in Fig. 7 for the same cylinders as in Sec. IV B. All data points correspond to pure transverse oscillations except for $L/W = 0.61$ and $D/H = 0.63$ in which case fluttering is superimposed. The frequency f is remarkably independent of the normalized diameter D/H, except for $D/H = 0.46$ and $L/W = 0.61$: in this case, f follows the common trend of variation for $V_{cx} > 0$ but its values are higher for $V_{cx} \leq 0$. The curves corresponding to $L/W = 0.22$ and $L/W = 0.61$ also coincide which generalizes the lack of dependence on L/W already observed for $D/H = 0.53$ (Fig. 6). Finally, fluttering does not induce any clear deviation from the common trend (⋈ symbols).

The amplitude of the transverse oscillations could not be measured quantitatively in the present experiments, even though they are detectable visually. In a previous work,[29] it was found to be generally independent of the velocity V_{cx} for a given cylinder and fluid. Moreover, the amplitude decreased as the diameter D increased: this could be expected since the global amplitude is generally of the order of the upper geometrical limit $H - D$.

C. Influence of the Reynolds number on the transverse oscillation frequency

All the experiments discussed above have been performed with the water-glycerol solution $WG10$: as shown above, the Reynolds number $Re^{loc} = V_r^{loc} H/\nu$ is then nearly independent of

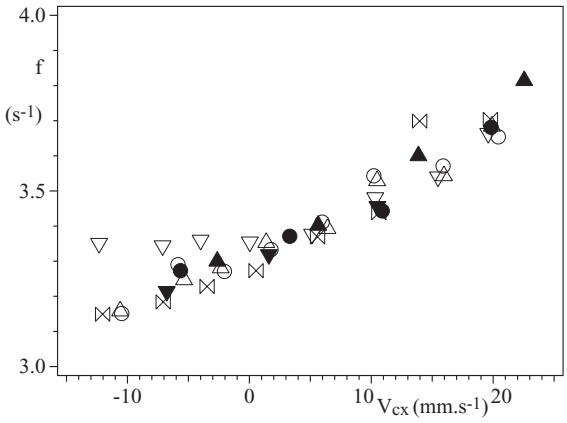

FIG. 7. Experimental variation of the transverse oscillation frequency as a function of the cylinder velocity V_{cx} for cylinders of different normalized diameters: $D/H = 0.46$ (▽, ▼), 0.53 (◯, ●), 0.56 (△, ▲), and 0.63 (⋈). Open symbols: $L/W = 0.61$; black symbols: $L/W = 0.22$. Flowing fluid: $WG10$ solution.

U and L/W for a given value of D/H. In order to study the influence of Re^{loc} on the transverse oscillations, it is necessary to vary the viscosity. Experiments have therefore been performed on a same cylinder using water and 6 water-glycerol solutions of different concentrations (see Table I). For three of the latter solutions, the density $\rho_f = 1.035$ g/cm^3 is kept constant by adding salt in order to study specifically the influence of the viscosity.

The corresponding variation of the Strouhal number $St^{loc} = f H/V_r^{loc}$ with Re^{loc} is plotted in Fig. 8 ($V_{cx} = 0$ in all cases): here, we estimate V_r^{loc} from the experimental variations of V_r as a function of L/W for $D/H = 0.53$ (Fig. 4) by assuming that the ratio V_r^{loc}/V_r for a given value of L/W is the same for all fluids of Table I.

Figure 8 shows that St^{loc} decreases by 25% as Re^{loc} varies from 15 to 30 and that all points follow the same trend independent of the density and the viscosity. This variation is very similar to that reported previously[28] for a tethered cylinder using either water or a nearly Newtonian water-natrosol solution (■, ▲ symbols): the values obtained in the free case are less than 10 % lower. In the tethered case, both the vertical motion and the variations of the roll angle are blocked: the removal of the corresponding kinetic energy components may therefore account for the slight increase of the

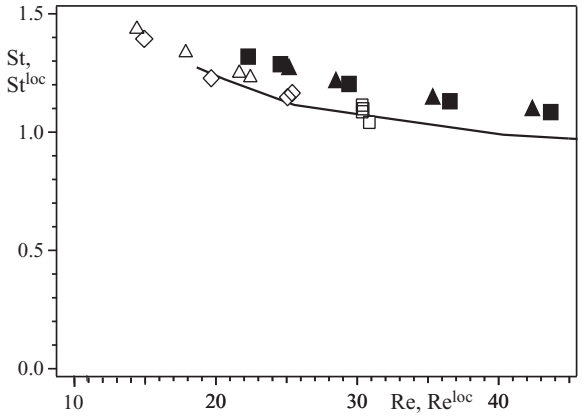

FIG. 8. Variations of the Strouhal number $St^{loc} = f H/V_r^{loc}$ of the oscillations of a free plexiglas cylinder ($L/W = 0.61$, $D/H = 0.53$) as a function of the Reynolds number $Re^{loc} = V_r^{loc} H/\nu$ for $V_{cx} = 0$ - (□): pure water (W); (◇): water-glycerol solutions (WG), and (△): water-salt-glycerol (WGS) solutions of concentrations 5%, 10%, and 15% (data points are in this order from right to left). Variation of $St = fH/U$ with $Re = UH/\nu$ for a tethered cylinder: $D/H = 0.64$, $L/W = 0.98$ using water (■) and a water-natrosol solution (▲) of viscosity 1.3×10^{-3} Pa s (from Ref. 28). Continuous line: numerical simulation.

frequency. There may also be an influence of the differences between the values of L/W and D/H. Numerical $2D$ simulations also reported in Ref. 28 display a very similar variation (continuous line).

Transverse oscillations obtained for free and tethered cylinders result then likely from the same physical mechanisms with only a small influence of the additional degrees of freedom.

VI. INFLUENCE OF THE CYLINDER LENGTH AND DIAMETER ON THE FLUTTERING INSTABILITY

As shown in Sec. III, the fluttering instability corresponds to oscillations of the angle θ of the cylinder with respect to the horizontal and to synchronous lateral oscillations of the center of mass (Figs. 3(c) and 3(d)). Fluttering takes place for large values of $D/H \geq 0.63$ either alone or superimposed onto transverse oscillations (Fig. 2). For $D/H = 0.53$, fluttering occurs, together with transverse oscillations, but only if $L/W = 0.89$ and $L/W = 0.95$. At the values of L/W still closer to 1 used in Ref. 29, sideways motions of the cylinder along z could only be of very small amplitude and the fluttering instability was not observable. For given geometrical ratios L/W and D/H, the occurrence of fluttering does not depend on the velocity U except for the longest cylinder ($L/W = 0.95$): in this case, fluttering only occurs at the largest upward flow velocities (⊠ symbols in Fig. 9).

As shown above using Figs. 4 and 5, the vertical drift of the cylinder does not seem to be influenced by the occurrence of the fluttering instability. More precisely, the slope β of the variation of V_{cx} with U is the same as in the regime of transverse oscillations; the global relative velocity V_r also follows the same trend of variation with L/W as for cylinders of same diameter in other regimes.

Figure 9 displays variations of the fluttering frequency f_f as a function of the velocity V_{cx} for several pairs of values of L/W and D/H. A first important feature is that f_f is at least 3 times lower than the frequency of transverse oscillations in similar geometries. Moreover, f_f is also constant with V_{cx} (and U) within experimental error for all values of L/W and D/H investigated (for transverse oscillations, the frequency increased instead slowly with V_{cx}).

Figure 10 shows that f_f decreases significantly with L/W, e.g., by a factor 3 as L/W increases from 0.22 to 0.9: this, too, differs from transverse oscillations for which f is independent of L/W at a given velocity V_{cx}. This strong dependence of f_f on L/W is not surprising since, unlike the transverse oscillations, the fluttering motion does not induce a $2D$ velocity field in the planes perpendicular to the cylinder axis. The bypass flows between the two ends of the cylinder and the side walls (Fig. 1(c)) will, in particular, influence strongly the fluttering process. Unlike its variation with L/W, the frequency f_f is, like f, nearly constant with the normalized diameter D/H: this is for instance visible in Fig. 10 for $L/W = 0.61$ and for dimensionless diameters $D/H = 0.63, 0.7, 0.77$

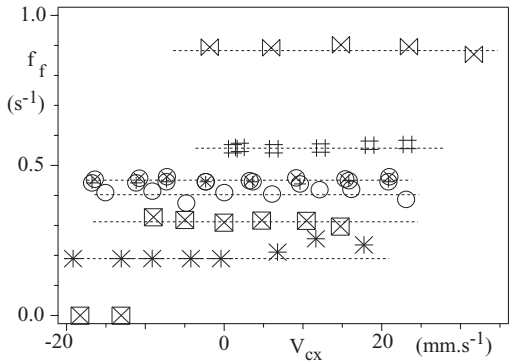

FIG. 9. Experimental variation of the fluttering frequency f_f for the $WG10$ solution as a function of the cylinder velocity V_{cx} for plexiglas cylinders of different normalized diameters: $D/H = 0.63$, $L/W = 0.22$ (⋈); $D/H = 0.77$, $L/W = 0.49$ (#); $D/H = 0.53$, $L/W = 0.89$ (✳); $D/H = 0.53$, $L/W = 0.94$ (⊠); $D/H = 0.63$, $L/W = 0.61$ (◯); $D/H = 0.7$, $L/W = 0.61$ (⊕); $D/H = 0.77$, $L/W = 0.61$ (⊗); and $f = 0$ means: no oscillation.

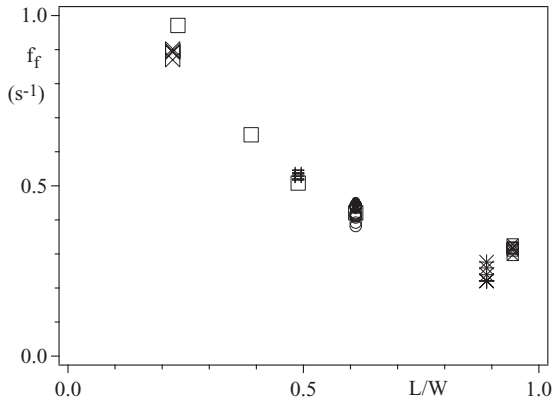

FIG. 10. Experimental variation of the fluttering frequency f_f with the normalized length L/W for cylinders with different normalized diameters and lengths: $D/H = 0.63$, $L/W = 0.22$ (▷◁); $D/H = 0.77$, $0.22 \leq L/W \leq 0.61$ (□); $D/H = 0.77$, $L/W = 0.49$ (#); $D/H = 0.53$, $L/W = 0.89$ (∗); $D/H = 0.53$, $L/W = 0.94$ (⊠); $D/H = 0.63$, $L/W = 0.61$ (◯); $D/H = 0.7$, $L/W = 0.61$ (⊕); and $D/H = 0.77$, $L/W = 0.61$ (⊗). Flowing fluid: $WG10$ solution.

((◯), (⊕) and (⊗) symbols). Similarly, for $L/W = 0.22$, the values of f_f corresponding to $D/H = 0.63$ and 0.77 are nearly equal.

It follows from these results that, unlike for transverse oscillations, the local relative velocity V_r^{loc} defined in Sec. IV A is likely not the relevant characteristic velocity for fluttering because it is constant with L/W while f_f varies. The global velocity V_r, instead, decreases linearly with L/W like f_f and is a better candidate; moreover, the corresponding Strouhal number St_f is practically constant when L/W increases from 0.23 to 0.61 with $St_f = 0.105 \pm 0.02$ for solution $WG10$ and $D/W = 0.77$ (f_f decreases from 0.85 to 0.45 s^{-1}). This suggests that V_r might be the relevant relative velocity for fluttering while V_r^{loc} is that for transverse oscillations. Further experiments using different cylinders and fluids are however needed to determine the dimensionless numbers controlling this instability.

Regarding the amplitude of the oscillations of δz_c and θ, these increase during the motion of the cylinder (starting from rest) and become constant with time and independent of the flow velocity U; the initial growth rate increases however with U. Moreover, the amplitude does not appear to depend on the ratio L/W: however, the ends of long cylinders ($L/W \gtrsim 0.6$) touch the sides during the oscillations which limits the amplitude of the variations of δz_c. Finally, the amplitude decreases when the fluid viscosity increases.

Visually, this fluttering instability resembles those of rectangular sheets falling obliquely.[25–27] However, such effects are observed in unconfined configurations while the frequency f_f of fluttering varies here with the lateral confinement (i.e., with L/W): it involves therefore likely a different mechanism in which viscous forces play an important part. A possible origin of fluttering is the dissymmetry of the flow created when the cylinder moves laterally so that $\delta z_c \neq 0$: then, the forces at its two ends are different, which creates a torque and a lateral force inducing respectively a variation of the tilt angle θ and a sideways motion.

VII. CONCLUSION

The present experimental study demonstrates that confinement may induce two different types of oscillatory instabilities of a free horizontal cylinder in a vertical viscous Hele-Shaw flow. Both the occurrence and the properties of these *transverse* and *fluttering* oscillations were shown to depend strongly and differently on the lateral and transverse confinement. Moreover, these instabilities may develop simultaneously and display novel specific features such as their onset at Reynolds numbers as low as 15, their lack of dependence on the cylinder diameter and the lack of influence of the cylinder length on the transverse oscillations.

The domain of observation of either type of instability is essentially determined by the transverse confinement parameter D/H. Transverse oscillations are typically observed for $0.4 \lesssim D/H \lesssim 0.6$ while fluttering occurs for $D/H \gtrsim 0.55$; there is therefore a domain in which the two kinds of oscillations

are superimposed but with no visible interaction between them. The lateral confinement L/W does not influence very much the onset of either instability: however, for $D/H = 0.53$, increasing L/W beyond 0.9 lets fluttering appear in addition to transverse oscillations. The occurrence of the fluttering instability does not influence significantly either the mean vertical velocity of the cylinder.

The frequency f of the transverse oscillations is remarkably constant with L/W down to $L/W \simeq 0.1$ for a given cylinder velocity V_{cx}: they appear therefore as a $2D$ process of characteristics independent of L/W. More precisely, one may assume a local $2D$ fluid velocity field around the cylinder with a relative velocity V_r^{loc} of the fluid and the cylinder independent of L/W, V_{cx} and of the distance z along the cylinder.

V_r^{loc} has a dominant influence and is the suitable characteristic velocity for defining the relevant Reynolds number $Re^{loc} = V_r^{loc} H/\nu$ for this instability: Re^{loc} is of the order of 20 for a 10% water-glycerol solution and for $0.46 \leq D/H \leq 0.56$. This value is significantly lower than the thresholds for vortex shedding behind cylinders between parallel planes (typ. 150−250): this confirms that one deals with a different process in which the coupling between the motion of the cylinder and the variations of the flow is a key factor. These transverse oscillations are similar to those observed for tethered cylinders in the same geometry:[28] the variations with Re^{loc} of the Strouhal number based on V_r^{loc} are indeed almost the same in both cases (for free cylinders, Re^{loc} is varied by using fluids of different viscosities).

Due to the two dimensional character of the transverse oscillations, their main features should be reproduced by $2D$ simulations of the type previously used for tethered cylinders.[28] These will allow us to understand better the origin of the weak dependence of the frequency f and of Re on the ratio D/H for which no simple explanation is presently available.

The fluttering oscillations have a very different dependence on the ratio L/W: their frequency f_f decreases indeed by a factor of 3 between $L/W = 0.22$ and $L/W = 1$ (however, like f, f_f does not depend on D/H). Unlike the transverse oscillations, fluttering depends therefore strongly on the clearance between the ends of the cylinder and the sides of the cell, as could be expected in view of the large displacements of the cylinder along z it induces. As a result, the *local* relative velocity V_r^{loc} which determines largely the transverse oscillations is not relevant for characterizing the fluttering process (f_f varies with L/W while V_r^{loc} remains constant). The global relative velocity V_r seems actually to be better adapted: the Strouhal number $St_f = f_f H/V_r$ based upon it St_f remains indeed constant within ±2% as L/W increases from 0.23 to 0.61 while V_r and f_f vary by a factor of 2. This hypothesis needs however to be confirmed by further experiments for other values of L/W and D/H and other viscosities μ.

Modeling thoroughly the fluttering motion would require $3D$ numerical simulations since flows both between the side of the cylinder (resp. its ends) and the walls of the cell (resp. its sides) are of importance. However, useful information may likely be obtained from a $2D$ numerical model, this time in the (x, z) plane, replacing the cylinder by a plane object (elongated rectangle for instance). Such simulations would take advantage of the specificity of Hele-Shaw cell flows (potential $2D$ mean flow in most of the surface of the cell) but friction forces in the region between the side of the cylinder and the cell walls would have to be included in the model. Further experimental studies, particularly of the influence of the viscosity and of the local structure of the flow will also be necessary to understand fully the mechanism of these instabilities and determine the relevant dimensionless parameters (particularly the Reynolds number) controlling this phenomenon.

ACKNOWLEDGMENTS

We thank B. Semin for his careful reading of the manuscript and his useful comments and J. E. Wesfreid for useful suggestions. We acknowledge the support of the RTRA Triangle de la Physique and of the LIA PMF-FMF (Franco-Argentinian International Associated Laboratory in the Physics and Mechanics of Fluids). M.V.D. acknowledges partial financial support from Universidad de Buenos Aires through its project UBACYT I403 and CONICET through its project PIP0410. M.V.D. was supported by a Bernardo Houssay grant allocated by the Argentinian and French ministries of research. We thank R. Pidoux for the realization of the experimental cell.

[1] H. Berthet, M. Fermigier, and A. Lindner, "Single fiber transport in a confined channel: Microfluidic experiments and numerical study," Phys. Fluids **25**, 103601 (2013); H. Berthet, "Single and collective fiber dynamics in confined microflows," Ph.D. thesis, UPMC, 2012.
[2] T. K. Guo, S. C. Zhang, B. Xiao, G. Q. Liu, F. Wang, J. C. Zhang, and X. B. Bian, "Evaluation and optimization of new nanocomposite fiber for fracturing technology based on a new equipment," Transp. Porous Media **94**, 243–257 (2012).
[3] E. Hurtig, S. Großwig, M. Jobmann, K. Kuhn, and P. Marschall, "Fibre-optic temperature measurements in shallow boreholes: Experimental application for fluid logging," Geothermics **23**, 355–364 (1994).
[4] J. S. Selker, L. Thévenaz, H. Huwald, A. Mallet, W. Luxemburg, N. van de Giesen, M. Stejskal, J. Zeman, M. Westhoff, and M. B. Parlange, "Distributed fiber optic temperature sensing for hydrologic systems," Water Resour. Res. **42**, W12202, doi:10.1029/2006WR005326 (2006).
[5] T. Read, O. Bour, V. Bense, T. Le Borgne, P. Goderniaux, M. V. Klepikova, R. Hochreutener, N. Lavenant, and V. Boschero, "Characterizing groundwater flow and heat transport in fractured rock using fiber-optic distributed temperature sensing," Geophys. Res. Lett. **40**, 2055–2059, doi:10.1002/grl.50397 (2013).
[6] M. V. D'Angelo, B. Semin, G. Picard, M. E. Poitzsch, J.-P. Hulin, and H. Auradou, "Single fiber transport in a fracture slit: Influence of the wall roughness and of the fiber flexibility," Transp. Porous Media **84**, 389–408 (2010).
[7] A. B. Richou, A. Ambari, and J. K. Naciri, "Drag force on a circular cylinder midway between two parallel plates at very low Reynolds numbers. Part 1: Poiseuille flow (numerical)," Chem. Eng. Sci. **59**, 3215–3222 (2004).
[8] A. B. Richou, A. Ambari, M. Lebey, and J. K. Naciri, "Drag force on a cylinder midway between two parallel plates at $Re \ll 1$. Part 2: Moving uniformly (numerical and experimental)," Chem. Eng. Sci. **60**, 2535–2543 (2005).
[9] B. Semin, J-P. Hulin, and H. Auradou, "Influence of flow confinement on the drag force on a static cylinder," Phys. Fluids **21**, 103604 (2009).
[10] J. H. Chen, W. G. Pritchard, and S. J. Tavener, "Bifurcation for flow past a cylinder between parallel planes," J. Fluid Mech. **284**, 23–41 (1995).
[11] L. Zovatto and G. Pedrizzetti, "Flow about a circular cylinder between parallel walls," J. Fluid Mech. **440**, 1–25 (2001).
[12] M. Sahin and R. G. Owens, "A numerical investigation of wall effects up to high blockage ratios on two-dimensional flow past a confined circular cylinder," Phys. Fluids **16**, 1305–1320 (2004).
[13] S. Camarri and F. Giannetti, "Effect of confinement on three-dimensional stability in the wake of a circular cylinder," J. Fluid Mech. **642**, 477–487 (2010).
[14] C. H. K. Williamson, "Vortex dynamics in the cylinder wake," Annu. Rev. Fluid. Mech. **28**, 477–539 (1996).
[15] C. H. K. Williamson and R. Govardhan, "A brief review of recent results in vortex-induced vibrations," J. Wind Eng. Ind. Aerodyn. **96**, 713–735 (2008).
[16] H. Faxén, "Forces exerted on a rigid cylinder in a viscous fluid between two parallel fixed planes," Proc. R. Swed. Acad. Eng. Sci. **187**, 1–13 (1946).
[17] A. S. Dvinsky and A. S. Popel, "Motion of a rigid cylinder between parallel plates in Stokes flow. Part 1: Motion in a quiescent fluid and sedimentation," Comput. Fluids **15**, 391–404 (1987).
[18] A. S. Dvinsky and A. S. Popel, "Motion of a rigid cylinder between parallel plates in Stokes flow. Part 2: Poiseuille and Couette flow," Comput. Fluids **15**, 405–419 (1987).
[19] E. Eklund and A. Jernqvist, "The motion of a neutrally buoyant circular cylinder in bounded shear flows," Chem. Eng. Sci. **49**, 3765–3772 (1994).
[20] H. H. Hu, "Motion of a circular cylinder in a viscous liquid between parallel plates," Theor. Comput. Fluid Dyn. **7**, 441–455 (1995).
[21] P. Ern, F. Risso, D. Fabre, and J. Magnaudet, "Wake-induced oscillatory paths of bodies freely rising or falling in fluids," Annu. Rev. Fluid. Mech. **44**, 97–121 (2012).
[22] P. Assemat, D. Fabre, and J. Magnaudet, "The onset of unsteadiness of two-dimensional bodies falling or rising freely in a viscous fluid: A linear study," J. Fluid Mech. **690**, 173–202 (2012).
[23] M. Chrust, G. Bouchet, and J. Dušek, "Numerical simulation of the dynamics of freely falling discs," Phys. Fluids **25**, 044102 (2013).
[24] F. Auguste, J. Magnaudet, and D. Fabre, "Falling styles of disks," J. Fluid Mech. **719**, 388–405 (2013).
[25] Y. Tanabe and K. Kaneko, "Behavior of a falling paper," Phys. Rev. Lett. **73**, 1372–1375 (1994).
[26] A. Belmonte, H. Eisenberg, and E. Moses, "From flutter to tumble, inertial drag and froude similarity in falling paper," Phys. Rev. Lett. **81**, 345–348 (1998).
[27] U. Pesavento and Z. J. Wang, "Falling paper: Navier-Stokes solutions, model of fluid forces, and center of mass elevation," Phys. Rev. Lett. **93**, 144501 (2004).
[28] B. Semin, A. Decoene, J. P. Hulin, M. L. M. Francois, and H. Auradou, "New oscillatory instability of a confined cylinder in a flow below the vortex shedding threshold," J. Fluid Mech. **690**, 345–365 (2012).
[29] M. V. D'Angelo, J. P. Hulin, and H. Auradou, "Oscillations and translation of a free cylinder in a viscous confined flow," Phys. Fluids **25**, 014102 (2013).